ChemComm

COMMUNICATION

View Article Online
View Journal | View Issue

Cite this: *Chem. Commun.*, 2024, **60**, 12185

Received 27th June 2024,
Accepted 14th August 2024

DOI: 10.1039/d4cc03144j

rsc.li/chemcomm

Isolation of a chloride-capped cerium polyoxo nanocluster built from 52 metal ions†

Anamar Blanes-Díaz,[a] Jennifer N. Wacker, ‡[a] Jennifer E. S. Szymanowski,[b] Jeffery A. Bertke [a] and Karah E. Knope *[a]

Four cerium compounds – $(HPy)_2[CeCl_6]\cdot 2(HPyCl)$ (Ce1-1), $(HPy)_2[CeCl_6]$ (Ce1-2), $(HPy)_m[Ce_{38}O_{56-x}(OH)_xCl_{50}(H_2O)_{12}]\cdot nH_2O$ (Ce38), and $(HPy)_m[Ce_{52}O_{80-x}(OH)_xCl_{59}(H_2O)_{17}]\cdot nH_2O$ (Ce52) – were crystallized from acidic aqueous solutions using pyridinium (HPy) counterions. The latter consists of two unique cerium oxide nanoclusters that are built from 52 metal ions and represents the largest chloride capped $\{Ce^{III/IV}O\}$ and/or $\{M^{IV}O\}$ (M = Ce, Th, U, Np, Pu) nanocluster that adopts the fluorite-type structure of MO_2 that has been reported.

Metal oxides are an important class of materials that have found applications ranging from catalysis to biomedicine.[1–4] Ceria, CeO_2, is one notable example as it is used in catalytic converters, glass polishing, solid-oxide fuel cells, oxygen sensing, alcohol oxidation, biomedical applications, and more.[5–8] This wide application space is engendered by the Ce^{3+}/Ce^{4+} redox-driven formation of highly reactive defect sites composed of oxygen vacancies and Ce^{3+} ions to form nonstoichiometric CeO_{2-x}.[5,8,9] Despite the pervasiveness of ceria-based materials, there is a need to better understand the behavior of bulk ceria for improved reactivity. One way to explore these structure–property relationships is through a molecular lens such as that afforded by cerium–oxo clusters. These species offer well-defined structural models that possess size-dependent properties and also provide insight into the chemical behavior of bulk CeO_2.[10–12] For example, Estevenon *et al.* recently demonstrated that Ce–oxo/hydroxo clusters, especially those of higher nuclearities (for example, $[Ce_{38}O_{54}(OH)_8(CH_3CH_2CO_2)_{36}(C_5H_5N)_8]$), could be used as platforms to understand cerium oxide nanomaterials.[13] Examination of the structural and electronic properties of Ce clusters and nanoparticles using high-energy-resolution fluorescence detection X-ray absorption spectroscopy (HERFD-XAS), high-energy X-ray scattering (HEXS), and single-crystal X-ray diffraction (SCXRD), showed an evolution in electronic structure as a function of cluster nuclearity, with $\{Ce_{38}\}$ most closely resembling the properties of CeO_2.[13] Motivated by these results as well as recent developments in the synthesis and structural chemistry of Ce–oxo clusters, broadly,[4,10,12–14] we sought to expand Ce–oxo cluster chemistry by leveraging outer coordination sphere interactions. We have isolated two novel cerium nanoclusters: $(HPy)_m[Ce_{38}O_{56-x}(OH)_xCl_{50}(H_2O)_{12}]\cdot nH_2O$ (**Ce38**) and $(HPy)_m[Ce_{52}O_{80-x}(OH)_xCl_{59}(H_2O)_{17}]\cdot nH_2O$ (**Ce52**) from acidic chloride solutions with pyridinium (HPy^{1+}) counterions. In addition, small changes to the reaction conditions in the presence of HPy^{1+} allowed for the isolation of monomeric species, $(HPy)_2[CeCl_6]\cdot 2(HPyCl)$ (**Ce1-1**) and $(HPy)_2[CeCl_6]$ (**Ce1-2**). Single crystal X-ray diffraction (SCXRD) was used to elucidate the structural chemistry of the compounds, and Raman and UV-vis-NIR spectroscopies were used to further characterize the isolated phases.

Dissolution of ceric ammonium nitrate in water followed by the addition of ammonium hydroxide resulted in precipitation of cerium hydroxide. The pellet was washed several times with water to remove ammonium. The yellow solid was then dissolved in dilute hydrochloric acid and utilized as a cerium source. Aliquots of pyridine were subsequently added to the Ce solution. Dark yellow crystals of **Ce1-1** and **Ce1-2**, yellow blocks of **Ce38**, and yellow parallelograms of **Ce52** were isolated at room temperature *via* solvent evaporation. The general synthetic approach follows that described for a $\{Ce_{38}\}$ nanocluster previously reported by our group,[14] but employs pyridinium counterions instead of potassium. Notably, the reaction reproducibly yielded four phases, **Ce1-1**, **Ce1-2**, **Ce38**, and **Ce52**, in various yields, with the reaction outcome strongly dependent on ambient conditions. In a typical synthesis, anywhere between 5–20 crystals of **Ce52** precipitated. Due to the limited

[a] *Department of Chemistry, Georgetown University, Washington, D.C. 20057, USA. E-mail: kek44@georgetown.edu*
[b] *Department of Civil & Environmental Engineering & Earth Sciences, University of Notre Dame, Notre Dame, IN 46556, USA*

† Electronic supplementary information (ESI) available: Synthesis, ORTEP, UV-vis-NIR and Raman spectra. CCDC 2359377–2359380. For ESI and crystallographic data in CIF or other electronic format see DOI: https://doi.org/10.1039/d4cc03144j

‡ Current address: Chemical Sciences Division, Lawrence Berkeley National Laboratory, Berkeley, CA, 94720, USA.

yields and co-precipitation of several phases, single crystals, rather than the bulk reaction product, were used for subsequent analyses. Full synthetic details are provided in the ESI.†

Single crystal X-ray diffraction studies revealed the formation of four different phases. **Ce1-1**, $(HPy)_2[CeCl_6]\cdot 2(HPyCl)$, and **Ce1-2**, $(HPy)_2[CeCl_6]$, consist of mononuclear $CeCl_6^{2-}$ anionic units. In both **Ce1-1** and **Ce1-2**, anionic $CeCl_6^{2-}$ complexes are charged balanced by two HPy^{1+} ions in the outer coordination sphere, with **Ce1-1** containing two additional $HPy^{1+}$and two Cl^{1-} ions in the second sphere. **Ce1-1** and **Ce1-2** were observed when the reaction solutions went to complete dryness. If the solution was not fully evaporated, **Ce38** and **Ce52** were observed. **Ce38** is related to previously reported chloride-capped $\{Ce_{38}\}$- and $\{An_{38}\}$–oxo clusters (An = U, Np, Pu).[14–16] It consists of a cluster core containing 38 Ce sites that is surface decorated by chloride ions and water molecules. Full structure descriptions of **Ce1-1**, **Ce1-2**, and **Ce38** are provided in the ESI.†

By comparison, **Ce52** is built from two discrete cerium-oxo nanoclusters, each containing 52 cerium atoms (Fig. 1). The compound crystallized in the monoclinic space group, $P2/m$, with the general formula $(HPy)_m[Ce_{52}O_{80-x}(OH)_xCl_{59}(H_2O)_{17}]\cdot nH_2O$. However, two crystallographically distinct $\{Ce_{52}\}$ clusters, $[Ce_{52}O_{80-x}(OH)_xCl_{60}(H_2O)_{16}]^{m-}$ and $[Ce_{52}O_{80-x}(OH)_xCl_{58}(H_2O)_{18}]^{m-}$, constitute the structure; as reflected in the formula, the clusters differ in the number of chloride and water molecules bound to the surface, and potentially the Ce^{III}/Ce^{IV} ratio. For simplicity, only one of the crystallographically unique clusters, $[Ce_{52}O_{80-x}(OH)_x$-$Cl_{60}(H_2O)_{16}]^{m-}$, is described in detail. The cluster core contains 52 cerium atoms bridged by μ_3- and μ_4-oxo anions layered in an $A:B:C:B:A$ (A = 6, B = 12, C = 16; based on Ce) pattern (Fig. S8, ESI†), with chloride and water ligands terminating the cluster surface. **Ce52** can be broken down into three structural units as shown in Fig. 1. Twenty-four Ce adopt the fluorite-type core of CeO_2. Within this $\{Ce_{24}\}$ subunit, ten of the Ce sites are eight coordinate, CeO_8, with the Ce bound exclusively to μ_3- and μ_4-oxo anions. The remaining fourteen Ce atoms are likewise eight-coordinate; however, these Ce are bound to either one or two water molecules along with oxo anions. Two $\{Ce_6\}$ and four $\{Ce_4\}$ subunits, shown in Fig. 1, complete the Ce_{52} cluster. Ce atoms in the $\{Ce_6\}$ and $\{Ce_4\}$ units are coordinated to both oxo and chloride anions, with each of the Ce atoms bound to four μ_3-/μ_4-oxo groups and four chlorides. The chlorides exhibit several coordination modes; there are two μ_2-, one μ_4-, and one terminal chloro group. Notably, the surface is chloride and water terminated. Average Ce-μ_3-O, Ce-μ_4-O, Ce–O_{H_2O} and Ce–Cl bond distances are 2.240(15) Å, 2.335(14) Å, 2.463(18) Å and 2.863(5) Å, respectively. The average Ce–O_{H_2O}, Ce-μ_3-O, and Ce-μ_4-O bond distances are consistent with those observed previously for a chloride-capped $\{Ce_{38}\}$.[14] However, the average Ce–Cl bond distance is longer than that reported for a chloride-terminated $\{Ce_{38}\}$, which exhibited a Ce–Cl range of 2.683(3)–2.713(3) Å.[14]

Overall, the $\{Ce_{52}\}$ cluster is anionic and, as such, protonated pyridinium cations reside in the outer coordination sphere. However, pyridinium ions could not be assigned during the crystal structure refinement due to disorder. Raman spectroscopic data were thus collected on a single crystal of **Ce52** (Fig. S13 and Table S12, ESI†). The spectrum was characterized by vibronic stretches indicative of pyridinium, with N–H stretches observed at 1600–1640 cm^{-1} and C–C stretches at approximately 1000 cm^{-1}. A split peak around 450 cm^{-1} can be attributed to Ce–O stretching modes; splitting is likely due to the presence of Ce-μ_3-O, Ce-μ_4-O, and potentially Ce-μ_3-OH within the cluster core.[14] Notably, for CeO_2, Ce–O stretching is typically observed around 465 cm^{-1}, and observation of the peaks around 450 cm^{-1} as well as a peak at 269.5 cm^{-1} is consistent with the Raman spectrum for CeO_2,[17] and underscore the similarities between **Ce52** and CeO_2. Peaks in the range of 200–400 cm^{-1} are consistent with Ce–Cl and Ce–O_{H_2O} modes.[14,18]

Bond valence summation (BVS) was used to determine the oxidation state of the Ce atoms in **Ce52** (Table S6, ESI†). Several Ce sites exhibited BVS values less than four, which may indicate

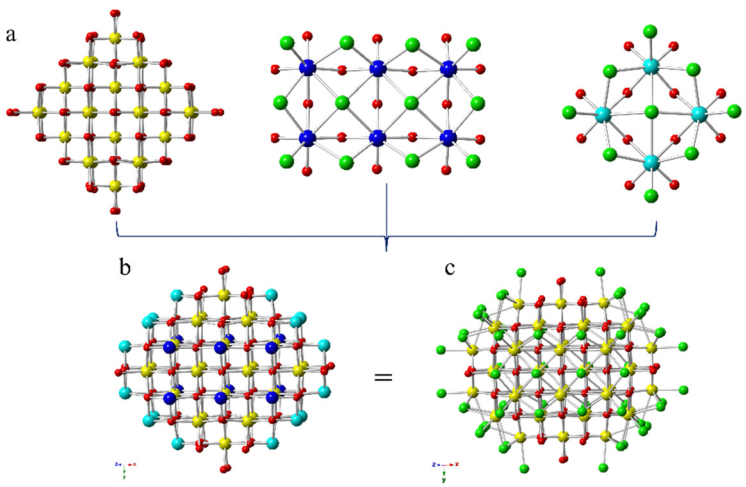

Fig. 1 Ball and stick representation of one of the crystallographically unique **Ce52** clusters illustrating (a) the $\{Ce_{24}\}$ (yellow), $\{Ce_6\}$ (dark blue) and $\{Ce_4\}$ (teal) subunits, and (b) the **Ce52** core, with the $\{Ce_{24}\}$, $\{Ce_6\}$, and $\{Ce_4\}$ units highlighted. Cl is in green, and O is in red. The chloride/water decorated **Ce52** cluster is shown in (c); all of the Ce sites are rendered as yellow spheres. Hydrogen atoms and disorder have been omitted for clarity.

some contribution from Ce^{III}. Formulation of the cluster as Ce^{III}/Ce^{IV} would be consistent with previously reported Ce nanoclusters. However, ambiguity in these assignments arises from uncertainty in the formulation of the μ_3-O sites as O^{2-} or OH^-, as well as the number of unresolved pyridinium molecules in the outer coordination sphere. It is also worth noting that recent work in polyoxovanadate clusters has shown that BVS values can deviate from assigned valence states due to delocalized electronic structure.[19] Additionally, there is some ambiguity in the experimentally determined BVS parameters for Ce as highlighted in the differences in BVS values calculated for both **Ce38** and **Ce52** using different BVS parameters (Tables S2–S8, ESI†).[20–22] Importantly, Ce–O parameters were recently redetermined.[21] This has not been done for Ce–Cl and thus, the assignment of the Ce oxidation state in **Ce52** is complicated by the fact that Cl ligands decorate the surface of the clusters.

Given the shortcomings of BVS, the oxidation state of the Ce sites in **Ce52** was evaluated by single-crystal UV-vis-NIR electronic absorption spectroscopy (Fig. S13, ESI†). The peak at approximately 1200 nm may be attributed to an intervalence charge transfer band and is consistent with Ce^{III}/Ce^{IV} in the structure.[14] Cerium complexes can exhibit signals in the UV and visible regions due to $4f^1 \rightarrow 5d^1$ transitions and ligand-to-metal charge transfer (LMCT) that can occur for Ce^{III} and Ce^{IV}, respectively. This is due to Ce^{III} being an f^1 metal and Ce^{IV} being an f^0 with no f → f transitions.[14,23] The UV-vis-NIR spectrum also displayed a band with a maximum around 400 nm. This band is likely attributed to LMCT based on literature precedence for halide-Ce^{IV} transitions.[14,23,24]

Based on BVS values and the electronic absorption spectrum, **Ce52** likely contains both Ce^{III}/Ce^{IV}. BVS values suggest that the Ce^{IV} sites are located at the center of the cluster and the possible Ce^{III} sites are located at the surface (Table S5, ESI†). Mixed valent Ce–oxo clusters have been previously reported. Examples include $\{Ce_{38}\}$, $\{Ce_{40}\}$, and $\{Ce_{100}\}$ clusters.[10,12] For $\{Ce_{40}\}$ and $\{Ce_{100}\}$, Ce^{III} were likewise located at the surface sites and specifically, on the (100) facet.[10,12] The presence of Ce^{III} at the surface of Ce–oxo clusters is likely attributed to the ease of formation of oxygen vacancies at the surface rather than in the core.[10]

Further bulk analysis of **Ce52** was complicated by low yields, and the isolation of the compound with other phases including **Ce38**, **Ce1-1**, and **Ce1-2** (Fig. 2); the latter consists of $CeCl_6^{2-}$ structural units. The isolation of various phases upon minor changes to the reaction conditions suggests that small differences in energy or solubility separate the formation of these compounds. Yet, the factors that push the reaction product to one phase over another remain unclear as solvent evaporation presumably impacts the concentration, pH, and ionic strength of the solution. Interestingly, **Ce52** and **Ce38** were observed when little solution was left, and **Ce1-1** or **Ce1-2** were isolated upon complete evaporation of the mother liquor. It is also worth noting that **Ce52** crystals left in solution would often redissolve and subsequently precipitate as **Ce38**.

Several Ce–oxo units ranging from $\{Ce_2\}$ to $\{Ce_{100}\}$ have been isolated to date, with $\{Ce_6\}$ being the most common cluster core reported for Ce.[10–12,14,25–36] These clusters vary in decoration; most are capped by organic ligands (*e.g.*, benzoic acid, propionic acid, and acetic acid), but inorganic anion (*e.g.*, chloride, sulfate) decorated clusters have also been observed.[4,10,11,14] Interestingly, clusters with nuclearities larger than $\{Ce_6\}$, including $\{Ce_{24}\}$, $\{Ce_{38}\}$, $\{Ce_{40}\}$ and $\{Ce_{100}\}$,[10,12] typically adopt the cubic, fluorite-type core of bulk CeO_2. Indeed, the **Ce38** and **Ce52** clusters reported here adopt the same fluorite-type structure. As mentioned previously, **Ce38** relates to previously reported $\{Ce_{38}\}$ clusters.[10,11,14] **Ce38** also parallels other $\{M_{38}\}$ clusters that have been reported for U, Np, and Pu.[15,16,37–40] In contrast to **Ce38**, no other $\{Ce_{52}\}$ or $\{An_{52}\}$ clusters that adopt the same core structure as **Ce52** described herein have been reported. For transition metal and lanthanide ions, including M = Pd, Au, Ti, Co, Cu, Ag, Eu, Nd, Pr, Gd, and Dy, $\{M_{52}\}$ clusters have been described.[41–48] However, these clusters adopt altogether different topologies than **Ce52**, and some are heterometallic, such as the $Eu_{52}Ni_{56-x}Cd_x$ cluster reported by Zheng *et al.*[48] Moreover, although Ce–oxo cluster chemistry literature has grown considerably over the past 10 years, there is a notable gap between $\{Ce_{40}\}$ and $\{Ce_{100}\}$. Furthermore, no inorganic ligated clusters larger than **Ce38** that adopt the fluorite-type structure of CeO_2 have been isolated. Density Functional Theory calculations have sought to examine the formation energies of single oxygen vacancies in $\{Ce_{44}\}$ and $\{Ce_{85}\}$, but importantly, no experimental data have been reported for these compounds.[49] As such, the synthesis and structural characterization of **Ce52** fills an important gap in our existing knowledge of Ce–oxo cluster chemistry and provides metrical information that may inform on important aspects of metal oxide and actinide chemistry, broadly.[15]

In summary, we report the synthesis of the largest known chloride-capped cerium cluster, $\{Ce_{52}\}$, along with a crystallographically unique $\{Ce_{38}\}$–oxo cluster and two $CeCl_6^{2-}$

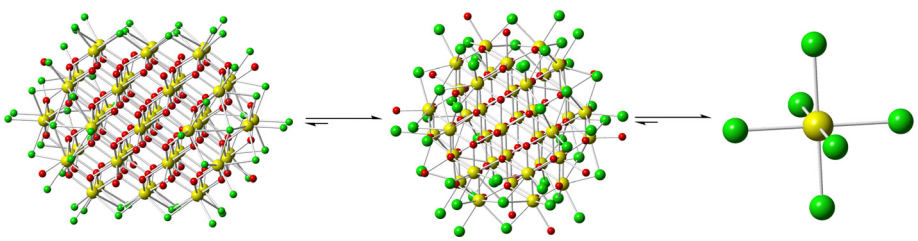

Fig. 2 Illustration of the structural units isolated *via* solvent evaporation: Ce_{52} (left), Ce_{38} (middle), and $CeCl_6^{2-}$ (right).

monomers. All of these units are anionic and contain pyridinium cations in the outer coordination sphere. Importantly, the **Ce52** cluster fills an important gap in our existing knowledge of Ce cluster chemistry. Isolation of this phase along with **Ce38** and $CeCl_6^{2-}$ *via* subtle changes to the reaction conditions suggests that small differences in energy, concentration, ionic strength, and/or solubility govern the formation and precipitation of these phases and warrant further examination. Aside from expanding Ce cluster chemistry itself, isolation of **Ce52** may also provide important insight (*i.e.*, synthetic parameters and metrical information) with which actinide clusters may be targeted and/or identified.

This work was supported by the U. S. Department of Energy, Office of Science, Office of Basic Energy Sciences, Early Career Research Program under Award DE-SC0019190.

Data availability

The data supporting this article including experimental details, crystallographic structure refinements, ORTEP diagrams, structure descriptions, and Raman and UV-vis-NIR spectroscopic data have been included as part of the ESI.† Crystallographic data for **Ce1-1**, **Ce1-2**, **Ce38**, and **Ce52** have been deposited at the CCDC under 2359377–2359380† and can be obtained from **https://www.ccdc.cam.ac.uk/structures/**.

Conflicts of interest

There are no conflicts to declare.

Notes and references

1 C. Wang, J. Yan, S. Chen and Y. Liu, *ChemPlusChem*, 2023, **88**, e202200462.
2 K. Zhou, G. Ding, C. Zhang, Z. Lv, S. Luo, Y. Zhou, L. Zhou, X. Chen, H. Li and S.-T. Han, *J. Mater. Chem. C*, 2019, **7**, 843–852.
3 D. Van den Eynden, R. Pokratath, J. P. Mathew, E. Goossens, K. De Buysser and J. De Roo, *Chem. Sci.*, 2023, **14**, 573–585.
4 I. Colliard, J. C. Brown and M. Nyman, *Inorg. Chem.*, 2023, **62**, 1891–1900.
5 J. Kašpar, P. Fornasiero and M. Graziani, *Catal. Today*, 1999, **50**, 285–298.
6 M. Flytzani-Stephanopoulos, *MRS Bull.*, 2001, **26**, 885–889.
7 G. M. Mullen, E. J. Evans, B. C. Siegert, N. R. Miller, B. K. Rosselet, I. Sabzevari, A. Brush, Z. Duan and C. Buddie Mullins, *React. Chem. Eng.*, 2018, **3**, 75–85.
8 B. Bhushan, S. Nandhagopal, R. Rajesh Kannan and P. Gopinath, *Colloids Surf., B*, 2016, **146**, 375–386.
9 P. Janoš, J. Ederer, V. Pilařová, J. Henych, J. Tolasz, D. Milde and T. Opletal, *Wear*, 2016, **362–363**, 114–120.
10 K. J. Mitchell, K. A. Abboud and G. Christou, *Nat. Commun.*, 2017, **8**, 1445.
11 M. C. Wasson, X. Zhang, K.-I. Otake, A. S. Rosen, S. Alayoglu, M. D. Krzyaniak, Z. Chen, L. R. Redfern, L. Robison, F. A. Son, Y. Chen, T. Islamoglu, J. M. Notestein, R. Q. Snurr, M. R. Wasielewski and O. K. Farha, *Chem. Mater.*, 2020, **32**, 8522–8529.
12 B. Russell-Webster, J. Lopez-Nieto, K. A. Abboud and G. Christou, *Angew. Chem., Int. Ed.*, 2021, **60**, 12591–12596.
13 P. Estevenon, L. Amidani, S. Bauters, C. Tamain, M. Bodensteiner, F. Meurer, C. Hennig, G. Vaughan, T. Dumas and K. O. Kvashnina, *Chem. Mater.*, 2023, **35**, 1723–1734.
14 J. N. Wacker, A. S. Ditter, S. K. Cary, A. V. Murray, J. A. Bertke, G. T. Seidler, S. A. Kozimor and K. E. Knope, *Inorg. Chem.*, 2022, **61**, 193–205.
15 L. Soderholm, P. M. Almond, S. Skanthakumar, R. E. Wilson and P. C. Burns, *Angew. Chem., Int. Ed.*, 2008, **47**, 298–302.
16 N. P. Martin, C. Volkringer, P. Roussel, J. Marz, C. Hennig, T. Loiseau and A. Ikeda-Ohno, *Chem. Commun.*, 2018, **54**, 10060–10063.
17 C. Schilling, A. Hofmann, C. Hess and M. V. Ganduglia-Pirovano, *J. Phys. Chem. C*, 2017, **121**, 20834–20849.
18 A. Brandt, Y. U. M. Kiselev and L. I. Martynenko, *ZAAC*, 2004, **474**, 233–240.
19 B. E. Petel, W. W. Brennessel and E. M. Matson, *J. Am. Chem. Soc.*, 2018, **140**, 8424–8428.
20 N. E. Brese and M. O'Keeffe, *Acta Crystallogr.*, 1991, **B47**, 192–197.
21 P. L. Roulhac and G. J. Palenik, *Inorg. Chem.*, 2003, **42**, 118–121.
22 A. Trzesowska, R. Kruszynski and T. J. Bartczak, *Acta Crystallogr., Sect. B: Struct. Sci.*, 2006, **62**, 745–753.
23 J. A. Bogart, A. J. Lewis, M. A. Boreen, H. B. Lee, S. A. Medling, P. J. Carroll, C. H. Booth and E. J. Schelter, *Inorg. Chem.*, 2015, **54**, 2830–2837.
24 J. L. Ryan and C. K. Jørgensen, *J. Phys. Chem.*, 1966, **70**, 2845–2857.
25 X. Wang, K. Brunson, H. Xie, I. Colliard, M. C. Wasson, X. Gong, K. Ma, Y. Wu, F. A. Son, K. B. Idrees, X. Zhang, J. M. Notestein, M. Nyman and O. K. Farha, *J. Am. Chem. Soc.*, 2021, **143**, 21056–21065.
26 M. Lammert, M. T. Wharmby, S. Smolders, B. Bueken, A. Lieb, K. A. Lomachenko, D. D. Vos and N. Stock, *Chem. Commun.*, 2015, **51**, 12578–12581.
27 K. J. Mitchell, J. L. Goodsell, B. Russell-Webster, U. T. Twahir, A. Angerhofer, K. A. Abboud and G. Christou, *Inorg. Chem.*, 2021, **60**, 1641–1653.
28 A. Bilyk, J. W. Dunlop, R. O. Fuller, A. K. Hall, J. M. Harrowfield, M. W. Hosseini, G. A. Koutsantonis, I. W. Murray, B. W. Skelton, A. N. Sobolev, R. L. Stamps and A. H. White, *Eur. J. Inorg. Chem.*, 2010, 2127–2152.
29 F. Yuan, Z. Gu, L. Li and L. Sha, *Polyhedron*, 2017, **133**, 393–397.
30 S. Banerjee, L. Huebner, M. D. Romanelli, G. A. Kumar, R. E. Riman, T. J. Emge and J. G. Brennan, *J. Am. Chem. Soc.*, 2005, **127**, 15900–15906.
31 I. L. Malaestean, A. Ellern, S. Baca and P. Kogerler, *Chem. Commun.*, 2012, **48**, 1499–1501.
32 S. L. Estes, M. R. Antonio and L. Soderholm, *J. Phys. Chem. C*, 2016, **120**, 5810–5818.
33 J. Jacobsen, B. Achenbach, H. Reinsch, S. Smolders, F.-D. Lange, G. Friedrichs, D. De Vos and N. Stock, *Dalton Trans.*, 2019, **48**, 8433–8441.
34 R. Das, R. Sarma and J. B. Baruah, *Inorg. Chem. Commun.*, 2010, **13**, 793–795.
35 L. Mathey, M. Paul, C. Coperet, H. Tsurugi and K. Mashima, *Chem. – Eur. J.*, 2015, **21**, 13454–13461.
36 M. P. Coles, P. B. Hitchcock, A. V. Khvostov, M. F. Lappert, Z. Li and A. Protchenko, *Dalton Trans.*, 2010, **39**, 6780–6788.
37 N. A. Vanagas, R. F. Higgins, J. N. Wacker, D. R. C. Asuigui, E. Warzecha, S. A. Kozimor, S. L. Stoll, E. J. Schelter, J. A. Bertke and K. E. Knope, *Chem. – Eur. J.*, 2020, **26**, 5872–5886.
38 L. Chatelain, R. Faizova, F. Fadaei-Tirani, J. Pecaut and M. Mazzanti, *Angew. Chem., Int. Ed.*, 2019, **58**, 3021–3026.
39 G. E. Sigmon and A. E. Hixon, *Chem. – Eur. J.*, 2019, **25**, 2463–2466.
40 C. Falaise, C. Volkringer, J. F. Vigier, A. Beaurain, P. Roussel, P. Rabu and T. Loiseau, *J. Am. Chem. Soc.*, 2013, **135**, 15678–15681.
41 A. Eichhöfer and D. Fenske, *J. Chem. Soc., Dalton Trans.*, 1998, **6**, 2969–2972.
42 W. H. Fang, L. Zhang and J. Zhang, *J. Am. Chem. Soc.*, 2016, **138**, 7480–7483.
43 Q. Lin, J. Li, Y. Dong, G. Zhou, Y. Song and Y. Xu, *Dalton Trans.*, 2017, **46**, 9745–9749.
44 H. D. Mai, P. Kang, J. K. Kim and H. Yoo, *Sci. Rep.*, 2017, **7**, 43448.
45 S. Zhuang, L. Liao, M.-B. Li, C. Yao, Y. Zhao, H. Dong, J. Li, H. Deng, L. Li and Z. Wu, *Nanoscale*, 2017, **9**, 14809–14813.
46 X. Zou, Y. Lv, X. Kang, H. Yu, S. Jin and M. Zhu, *Inorg. Chem.*, 2021, **60**, 14803–14809.
47 E. G. Mednikov, S. A. Ivanov, I. V. Slovokhotova and L. F. Dahl, *Angew. Chem., Int. Ed.*, 2005, **44**, 6848–6854.
48 R. Chen, Z. H. Yan, X. J. Kong, L. S. Long and L. S. Zheng, *Angew. Chem., Int. Ed.*, 2018, **57**, 16796–16800.
49 C. Loschen, A. Migani, S. T. Bromley, F. Illas and K. M. Neyman, *Phys. Chem. Chem. Phys.*, 2008, **10**, 5730–5738.

